RSC Advances

PAPER

View Article Online
View Journal | View Issue

Cite this: *RSC Adv.*, 2023, **13**, 10384

Multifunctional fluorescent Eu-MOF probe for tetracycline antibiotics and dihydrogen phosphate sensing and visualizing latent fingerprints†‡

Theanchai Wiwasuku,[ae] Adulvit Chuaephon,[b] Theerapong Puangmali,[b] Jaursup Boonmak,*[a] Somlak Ittisanronnachai,[c] Vinich Promarak[d] and Sujittra Youngme[a]

The contamination of tetracycline antibiotics and dihydrogen phosphate ($H_2PO_4^-$) in food and the environment is one of the major concerns for human health. Herein, a water-stable carboxyl-functionalized europium metal–organic framework (**Eu-MOF**) was prepared and demonstrated, for the first time, as a dual-responsive fluorescent sensor of tetracycline antibiotics (oxytetracycline (OTC), tetracycline (TC), and doxycycline (DOX)) and $H_2PO_4^-$ *via* fluorescent turn-on and turn-off, respectively. **Eu-MOF** presents a sensitive and selective detection of OTC with a rapid response time (1 min) and good anti-interference ability. The limits of detection (LODs) of 78 nm, 225 nm, and 201 nM were achieved for OTC, TC, and DOX, respectively. Coordination and hydrogen bonding led to energy and electron transfer from the TC to the MOF, contributing to the fluorescent enhancement mechanism. Moreover, **Eu-MOF** can effectively detect $H_2PO_4^-$ *via* fluorescence turn-off with a LOD of 0.70 μM. The interactions between $H_2PO_4^-$ and MOF interrupt the energy transfer from ligand to MOF, leading to fluorescence quenching. In addition, **Eu-MOF** was successfully applied to determine OTC and $H_2PO_4^-$ in real samples, obtaining satisfactory recoveries and RSDs. More fascinating, **Eu-MOF** could be utilized to develop latent fingerprints on various surfaces, providing well-defined fluorescent fingerprint details in which the sweat pores can be seen with the naked eye.

Received 6th January 2023
Accepted 2nd March 2023

DOI: 10.1039/d3ra00100h

rsc.li/rsc-advances

1. Introduction

Antibiotic drugs and inorganic pollutants are being discharged at an extremely high rate from industrial and other sources into the environment, leading to one of the most concerning human health and environmental issues. In particular, tetracycline antibiotics (TCs) (oxytetracycline (OTC), tetracycline (TC), and doxycycline (DOX)) are a family of broad spectrum antibiotics used in animal, aquaculture, and human infection therapy.[1] TCs residues have been found in food products such as meat, fish, milk, and honey.[2] Long-term exposure and accumulation of tetracycline antibiotics cause undesirable effects to human health such as anaphylactic reaction, gastrointestinal disturbance, and hepatotoxicity and promote bacterial resistance to antibiotics.[3–5] At the same time, inorganic phosphate is an essential nutrient for the human body that has both excess and deficiency-related deleterious health effects. For example, excess $H_2PO_4^-$ ions in the blood can induce a variety of disorders, including hypocalcaemia, which causes increased neuronal excitability, tetany, and convulsions, as well as obstructing numerous biological functions.[6] An excessive level of phosphate can also cause serious environmental problems such as eutrophication.[7,8] The contamination of this toxic anion in drinking water and environmental water is mostly due to the extensive use of agrochemicals, industrial waste, and inferior agricultural techniques.[9] The detection of phosphate ions is quite challenging and important for water quality monitoring. Therefore, it is essential to develop an efficient, practical, and dependable detection method for TCs and inorganic phosphate. The fluorescent method has attracted extensive attention in sensing applications due to its high sensitivity, specificity, quick response, and simplicity of use.[10]

[a]*Materials Chemistry Research Center and Center of Excellence for Innovation in Chemistry, Department of Chemistry, Faculty of Science, Khon Kaen University, Khon Kaen, 40002, Thailand. E-mail: jaursup@kku.ac.th*

[b]*Department of Physics, Faculty of Science, Khon Kaen University, Khon Kaen 40002, Thailand*

[c]*Frontier Research Center (FRC), Vidyasirimedhi Institute of Science and Technology, Rayong, 21210, Thailand*

[d]*Department of Materials Science and Engineering, School of Molecular Science and Engineering, Vidyasirimedhi Institute of Science and Technology, Rayong, 21210, Thailand*

[e]*Functional Materials and Nanotechnology Centre of Excellence, Walailak University, Nakhon Si Thammarat, 80160, Thailand*

† This work is dedicated to Professor Sujittra Youngme, Khon Kaen University, Thailand, on the occasion of her retirement.

‡ Electronic supplementary information (ESI) available. See DOI: https://doi.org/10.1039/d3ra00100h

In recent years, numerous metal–organic frameworks (MOFs), which are hybrid porous crystalline materials made up of organic ligands and metal ions, have been explored as fluorescent sensors for environmental contaminants such as antibiotics, explosives, anions, cations, and dyes.[11–15] This is because they have tuneable functional sites and pore surfaces, viable supramolecular interactions between the target analytes and host frameworks, a large surface area, excellent stability, and the ability for regeneration. Among MOF-based fluorescent sensors, lanthanide MOFs (Ln-MOFs) have received interest due to their exceptional antenna-effect optical features, such as substantial Stokes shifts, visible fluorescent intensity, and great colour purity.[16] Fluorescent MOFs have been reported for the efficient sensing of several types of TCs.[17–20] Most of them were employed for TCs detection based on turn-off resulting from the energy or electron transfer between the sensor and the analyte. However, a few turn-on type fluorescent sensors for TCs detection have been reported.[21–23] Notably, the functional group (*e.g.*, $-NH_2$ and –COOH) acts as a possible site of interaction with organo-analytes and possesses recognition ability in MOFs.[24,25] For instance, amino group in NH_2-MIL-53(Al) demonstrates favourable selectivity due to the synergistic effect of the electron transfer and the high absorption of TCs at the excitation energy of MOFs, leading to turn-off effect.[5] As far as we know, Ln-MOF containing free –COOH functional groups for the detection of oxytetracycline based on fluorescent enhancement has not been explored. Besides, the detection of phosphate ions in aqueous solution is challenging due to their powerful hydration effect, which requires a strong affinity between the recognition sites and the analytes.[26] The sensor probe must be stable and require appropriate detecting sites in the water. According to the literature, MOF-based dihydrogen phosphate detection reports have been seldom documented.[9,27,28] Previous MOFs had good detection capability but limited water stability and a high limit of detection, limiting their practical applications. To overcome these limitations, designing a water-stable MOF fluorescent sensor for TCs and dihydrogen phosphate with high sensitivity and selectivity is challenging. To the best of our knowledge, there is no report on the dual-functions of fluorescent sensors for the detection of TCs and $H_2PO_4^-$ based on MOF.

In addition, fingerprints are unique, remain relatively unchanged throughout a person's life, and leave imprints when touched.[29] In many cases, the mark of latent fingerprints (LFPs) is not visible to the naked eye at crime scenes, but can be disclosed through visualization for the purposes of forensic investigation and individual identification. For the identification of LFPs up till now, several approaches have been proposed.[30–34] It is still challenging to develop a novel method for visualizing LFPs that has the advantages of being quick, accurate, sensitive, and having distinct microscopic properties. Lanthanide-based MOFs have the potential to significantly enhance the contrast and sensitivity of conventional visualization techniques by combining a good fluorescence feature of the lanthanide core with an active site of an organic ligand for binding with LFPs residues. Up to date, only few MOFs have been reported for imaging LFPs.[35,36] Therefore, it is necessary to establish and expand an efficient technique employing MOF for fingerprint development in practical application in the forensic science area.

In light of this, a highly water-stable **Eu-MOF** has been designed and synthesized using 1,2,4,5-benzenetetracarboxylic acid (H_4btec) as a linker by a one-pot hydrothermal method. The structure of **Eu-MOF** contains intriguing uncoordinated carboxyl (–COOH) groups to act as a active site for the target molecules. Notably, **Eu-MOF** demonstrated exceptional water stability and acid-base tolerance (pH = 2–14). The use of **Eu-MOF** as a dual functional fluorescence sensor for detecting tetracycline antibiotics (OTC, TC, and DOX) and dihydrogen phosphate ($H_2PO_4^-$) has been demonstrated. It displayed an impressive fluorescent enhancement for tetracycline antibiotics even in the presence of other interference. In particular, **Eu-MOF** exhibited fast recognition of OTC with a quick response time of 1 min, excellent anti-interfering ability, and a low limit of detection (LOD) (78 nM). The LODs of TC and DOX were found to be 225 nM and 201 nM, respectively. The fluorescent enhancement process was primarily based on hydrogen bond and coordination interaction that led to energy and electron transfer from antibiotics to MOF. In addition, **Eu-MOF** could sensitively and selectively detect $H_2PO_4^-$ among various anions based on a fluorescence quenching assay. Limit of detection of $H_2PO_4^-$ was calculated to be 0.70 μM. The quenching mechanism is attributed to the obstruction of an energy transfer from ligand to Eu^{3+} centre in MOF because of the interaction between the anion and the sensor. Furthermore, the proposed material was successfully applied for the determination of OTC and in real samples with acceptable recoveries, supporting the possible application of **Eu-MOF** in the detection of toxic substances in real samples. More fascinating, **Eu-MOF** could be employed as a fluorescent material for identifying of fingerprints on various substrates, which is a very promising approach for fingerprint visualization in forensic investigation.

2. Experimental

2.1 Materials and physical measurements

All reagents were purchased commercially and used as received. FT-IR spectra were collected at 4000–600 cm^{-1} on a Bruker Tensor 27 spectrophotometer with a Pike ATR cell. The elements of C, H, and N were analysed with a PerkinElmer PE 2400CHNS. Shimadzu UV 2450 was used to record UV-vis spectra in solution. Powder X-ray diffraction (PXRD) measurement was performed with Cu Kα radiation at 2θ range of 5–50° on Bruker D8 ADVANCE. Fluorescent spectrum was collected on Spectrofluorometer FS5 Edinburgh at room temperature. X-Ray Photoelectron Spectroscopy (XPS) was recorded on JEOL JPS-9010 MC with a Twin anode (Mg Kα source, 1253.6 eV and Al Kα source, 1486.6 eV) at 12 kV and 25 mA. Absolute photoluminescence quantum yield measurement in solid state was carried out using Edinburgh Instruments FLS980 spectrometer integrated with a calibrated integrating sphere.

2.2 Hydrothermal synthesis of Eu-MOF

In a hydrothermal tube, $Eu(NO_3)_3 \cdot 5H_2O$ (0.1 mmol, 0.0435 g) and H_4btec (0.1 mmol, 0.0254 g) were dissolved in 5 mL of DI water. The solution was then heated for 12 hours at 120 °C, and the reaction was cooled to room temperature. The colorless-block crystals were obtained at a 53% yield (based on metal salt). The resulting sample was separated and washed with DI water. CHN anal. calcd (%) for $C_{20}H_{16}Eu_2O_{21}$ (M_r = 896.26 g mol^{-1}): C, 26.80 and H, 1.80%. Found (%): C, 26.34 and H, 1.78%. Selected IR peak (cm^{-1}): ν_s(OH) = 3486w and 3410w, ν_{as}(OCO) = 1667 s and 1540 s, ν_s(OCO) = 1495 s and 1379 s.

2.3 Detection of oxytetracycline

For the quantitative detection of OTC, various quantities of OTC were added to a 5 mL volumetric flask containing 1 mL of water-suspended **Eu-MOF** (0.2 mg mL^{-1}). The mixed solution was further diluted to a volume of 5.00 mL to get a final concentration of OTC between 0 and 25 μM. The emission spectra of the solutions were measured with the excitation wavelength at 368 nm after 10 minutes. To investigate the effects of coexisting substances on the selective detection of OTC by **Eu-MOF**, 25 μM antibiotics (amox icillin, penicillin G, and streptomycin), amino acids (histidine, lysine, phenylalanine, and aspartic acid), and physiological substances (uric acid, urea, ascorbic acid, sucrose, glucose, lactose, and glutathione) were added to a solution of **Eu-MOF** containing 25 μM of OTC. After 10 minutes, the fluorescence intensities at 616 nm were measured to determine the effect of coexisting compounds on the OTCs ability for selective determination.

2.4 Detection of $H_2PO_4^-$

In a 5 mL volumetric flask, 1 mL of water-suspended **Eu-MOF** (0.2 mg mL^{-1}) was mixed with 25 μL of 10 mM anionic aqueous solution. The tested anions consist of F^-, Cl^-, Br^-, I^-, NO_3^-, CO_3^{2-}, NO_2^-, CN^-, OAc^-, ClO_4^-, SO_4^{2-}, S^{2-}, and $H_2PO_4^-$ in term of sodium salts. The mixed solution was diluted to 5.00 mL to get 50 μM of anion. The fluorescence spectra were recorded at 254 nm after 30 min at ambient temperature.

2.5 Detection of OTC and $H_2PO_4^-$ in real samples

Whole fresh milk, UHT milk, chicken breast, and honey samples were used to determine the presence of OTC. The fresh milk was obtained from Khon Kaen University's dairy shelf. UHT milk, chicken breast, and honey were bought from a supermarket in Khon Kaen, Thailand. Milk samples were prepared according to the reported work with modification,[37] 1 mL of milk was deproteinized and defatted in 3 mL of methanol and 1 mL of 1% (v/v) acetic acid. The solution was vortexed for 2 minutes and centrifuged for 10 minutes at 6000 rpm. Supernatant was filtered through a 0.45 m membrane (VertiClean™ NYLON) and diluted to 100 mL. The honey sample was prepared in accordance with the reported work, with modifications.[38] 2 g of honey was diluted to 10 mL of DI water. The mixture was vortexed for 2 minutes, filtered using a 0.45 μm membrane filter (VertiClean™ NYLON) and diluted to 100 mL. A sample of chicken breast was prepared with some modifications from the literature.[39] 5.00 g chicken breast was cut into small pieces and mixed with 5 mL of acetonitrile : H_2O (70 : 30, v/v). The mixture was homogenized for 5 min, and then centrifuged for 10 min at 4000 rpm. Using a 0.45 μm membrane filter (VertiClean™ NYLON), the supernatant was filtered before being diluted to 100 mL. Two water samples (drinking water and lake water) were selected for the determination of $H_2PO_4^-$. They were prepared by filtration through a 0.45 μm membrane filter (VertiClean™ NYLON) and then tested directly after filtration.

2.6 Development and imaging of latent fingerprints

The fingerprint donor was required to wash his hands with soap and water and run his fingers across his forehead and gently press them on several substrates, including glass, paper, and plastic. Finely ground **Eu-MOF** powders were sprinkled onto the LFPs and the brush was then used to remove the unnecessary particles. The photographs of the developed fingerprints were taken under UV light (365 nm) using a smartphone.

3. Results and discussion

3.1 Synthesis and characterization of water-stable Eu-MOF

The typical synthesis of **Eu-MOF** as a water-stable fluorescent sensor for oxytetracycline and $H_2PO_4^-$ sensing and visualization of LFPs was illustrated in Fig. 1. **Eu-MOF** was successfully prepared from the mixture of europium nitrate and H_4btec ligand under a one-pot green hydrothermal reaction. As shown in Fig. S1,‡ the PXRD pattern of **Eu-MOF** is identical to the simulated pattern of reported Tb-MOF, namely $[Tb_2(H_2\text{-btec})(btec)(H_2O)] \cdot 4H_2O$, according to CCDC no. 2142666.[40] This confirms that the prepared **Eu-MOF** is structurally identical to the reported Tb-MOF and is in pure phase. Taking the crystal structure of Tb-MOF as a representative, the three-dimensional structure of Tb-MOF consists of the Tb^{3+} centre which is nine-coordinated by carboxylate groups of ligand and water molecule. As shown in Fig. S2(a),‡ neighbouring Tb^{3+} centres are connected by carboxyl oxygen atoms of the ligand to create 1D zigzag chains. Each chain is linked to the adjacent chains by a μ_6-bridging $btec^{4-}$ ligand to create a 2D layer. The 2D layers are connected further with H_2btec^{2-} ligands, resulting in a 3D structure containing 1D channels with respective diameter of 9.892 × 10.433 $Å^2$. In the channel, the lattice water molecules and free carboxyl groups (–COOH) from H_2btec^{2-} ligand are free. According to the crystal structure of Tb-MOF, two kinds of carboxylate ligands, H_2btec^{2-} and $btec^{4-}$ in **Eu-MOF**, that have different coordination natures are concluded (Fig. S2(b and c)‡). As presented in Fig. S3,‡ the IR peaks at 3401 and 3486 cm^{-1} of **Eu-MOF** are attributed to –OH stretching. The observation of an IR peak at 1667 cm^{-1} indicates the presence of free –COOH groups in H_2btec^{2-}. The vibrations of the carboxylate groups were observed at 1610 cm^{-1}, 1540 cm^{-1}; 1495 cm^{-1}, 1379 cm^{-1} are attributed to different $\nu_{as}(COO^-)$ and $\nu_s(COO^-)$ stretching vibrations of the coordinated carboxylate groups, which also suggests the different coordination modes of the carboxylate groups (bidentate chelating and bidentate bridging).

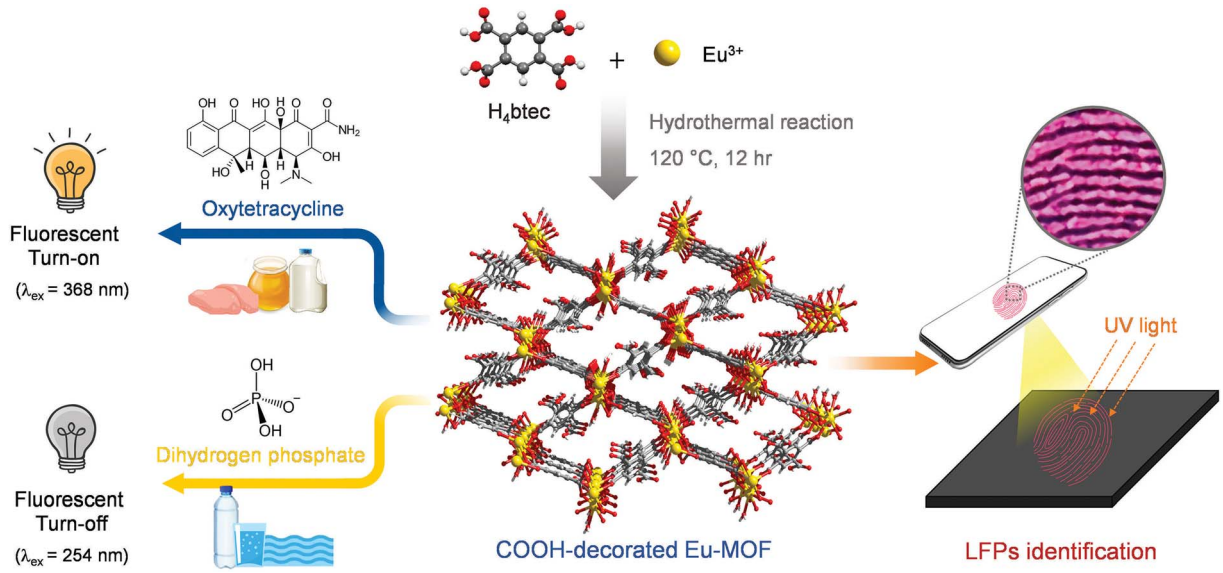

Fig. 1 Scheme diagram for synthesis of water-stable **Eu-MOF** and its application for the detection of oxytetracycline and $H_2PO_4^-$ and visualization of latent fingerprints (LFPs).

3.2 Water stability and fluorescent property of Eu-MOF

The chemical stability of **Eu-MOF** was examined. As shown in Fig. 2(a), the PXRD patterns of **Eu-MOF** soaked in DI and boiling water, are similar to those of the synthesized compound. The stability of **Eu-MOF** in acidic and basic solutions was also studied. All XRD patterns of the treated sample after 12 hours in aqueous solutions with pH values ranging from 2 to 12 are in good agreement with the pristine pattern (Fig. 2(a)). These results reveal the great water stability and acid-base resistance of **Eu-MOF** which is a precondition for the development of functional materials with practical applications. At room temperature, the solid state fluorescent characteristics of H_4btec and **Eu-MOF** were investigated. As shown in Fig. 2(b), upon stimulation at 280 nm, the H_4btec ligand exhibited an emission peak at 330 nm due to the π–π transition. When excited at 254 nm, the spectrum of **Eu-MOF** demonstrated the strong characteristic fluorescence of Eu^{3+} with emission peaks at 592, 616, 650, and 698 nm, which were attributed to the typical f–f transitions of Eu^{3+}, namely, $^5D_0$–$^7F_1$, $^5D_0$–$^7F_2$, $^5D_0$–$^7F_3$, and $^5D_0$–$^7F_4$, respectively. The relative intensities of several electronic transitions and the band splitting were influenced by the local symmetry of the Eu^{3+} crystal field. The strongest red emission at 616 nm is attributed to the transition of $^5D_0$-$^7F_2$ generated by electric dipole transition. This emission is hypersensitive to the coordination environment, resulting in the bright red narrow sharp emission. The quantum yields of **Eu-MOF**-based probe were observed to be of 30% and 13% at excitations of 254 nm and 368 nm, respectively. Thus, under UV light irradiation, **Eu-MOF** emitted a red fluorescence (the inset of Fig. 2(b)). The fluorescent emission of H_4btec ligand in **Eu-**

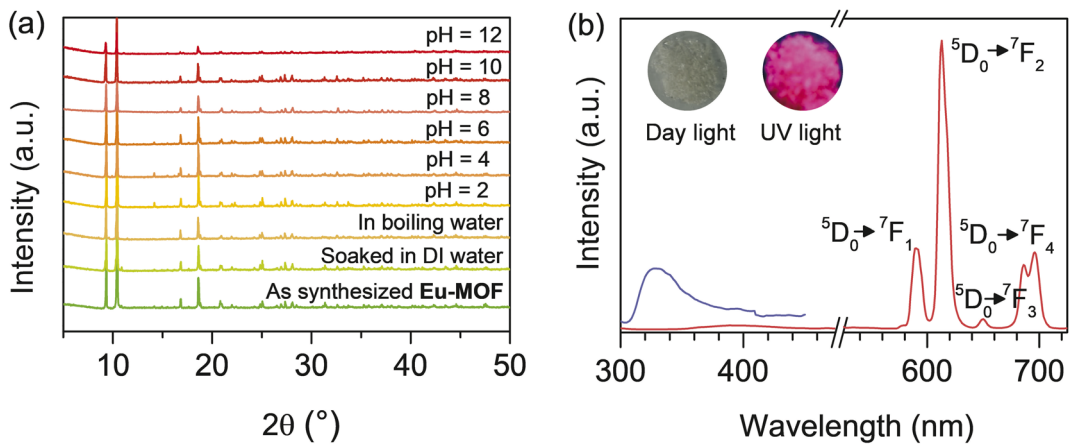

Fig. 2 (a) PXRD patterns of untreated **Eu-MOF** and treated **Eu-MOF** in different conditions. (b) Solid-state fluorescent spectrum of **Eu-MOF** (red line, $\lambda_{ex} = 254$ nm) and free H_4btec ligand (blue line, $\lambda_{ex} = 280$ nm) at room temperature. The inset show visual color of **Eu-MOF** under day light and UV light.

MOF is relatively low, indicating the energy transfer from ligand to Eu^{3+}.[41] Because there are a variety of application conditions, the pH stability of the sensor in various solutions is also important. Therefore, the effect of pH on the fluorescent intensity of **Eu-MOF** was investigated. As shown in Fig. S4,‡ when the pH ranged from 5 to 9, a strong fluorescent intensity was still detected. The results indicated that **Eu-MOF** exhibited good water and fluorescence stability, which indicated its potential as a good chemical sensor.

3.3 Turned-on detection of OTC

According to the good fluorescence and excellent water durability of **Eu-MOF**, its potential for detecting antibiotics in water was investigated. Various antibiotics (oxytetracycline (OTC), tetracycline (TC), doxycycline (DOX), amoxicillin, penicillin G, and streptomycin), amino acids (histidine, lysine, phenylalanine, and aspartic acid), uric acid, urea, ascorbic acid, sucrose, glucose, lactose, and glutathione were selected to demonstrate the fluorescent sensing of **Eu-MOF**. The chemical structures of antibiotics are given in Fig. S5.‡ As shown in Fig. 3(a and b), in the presence of various substances, **Eu-MOF** exhibits a considerable increase in emission intensity only in the presence of tetracycline-class antibiotics (OTC, DOX, and TC). Obviously, OTC exhibits a greater change than other tetracycline-like antibiotics. This revealed that the **Eu-MOF** could selectively identify these tetracycline-like antibiotics, especially OTC. Thus, OTC was chosen as the representative to carry out a certain analysis. The spectrum responses of the **Eu-MOF** probe to different OTC concentrations are shown Fig. 3(c). Notably, the emission intensity at 616 nm increases steadily in proportion to the amount of OTC added. The fluorescence intensity exhibits a good linear association ($R^2 = 0.998$) with the OTC concentration in the range of 2.5–15 μM (Fig. 3(d)). The limit of detection (LOD) was calculated to be 0.078 μM (LOD = $3\sigma/S$ (σ = a standard deviation of the fluorescent test for 10 blank solutions; S = slope of the calibration curve)). Furthermore, fluorescent titration experiments were used to quantitatively determine DOX and TC. As shown in Fig. S6(a and c),‡ the fluorescent intensity of **Eu-MOF** was increased with increasing

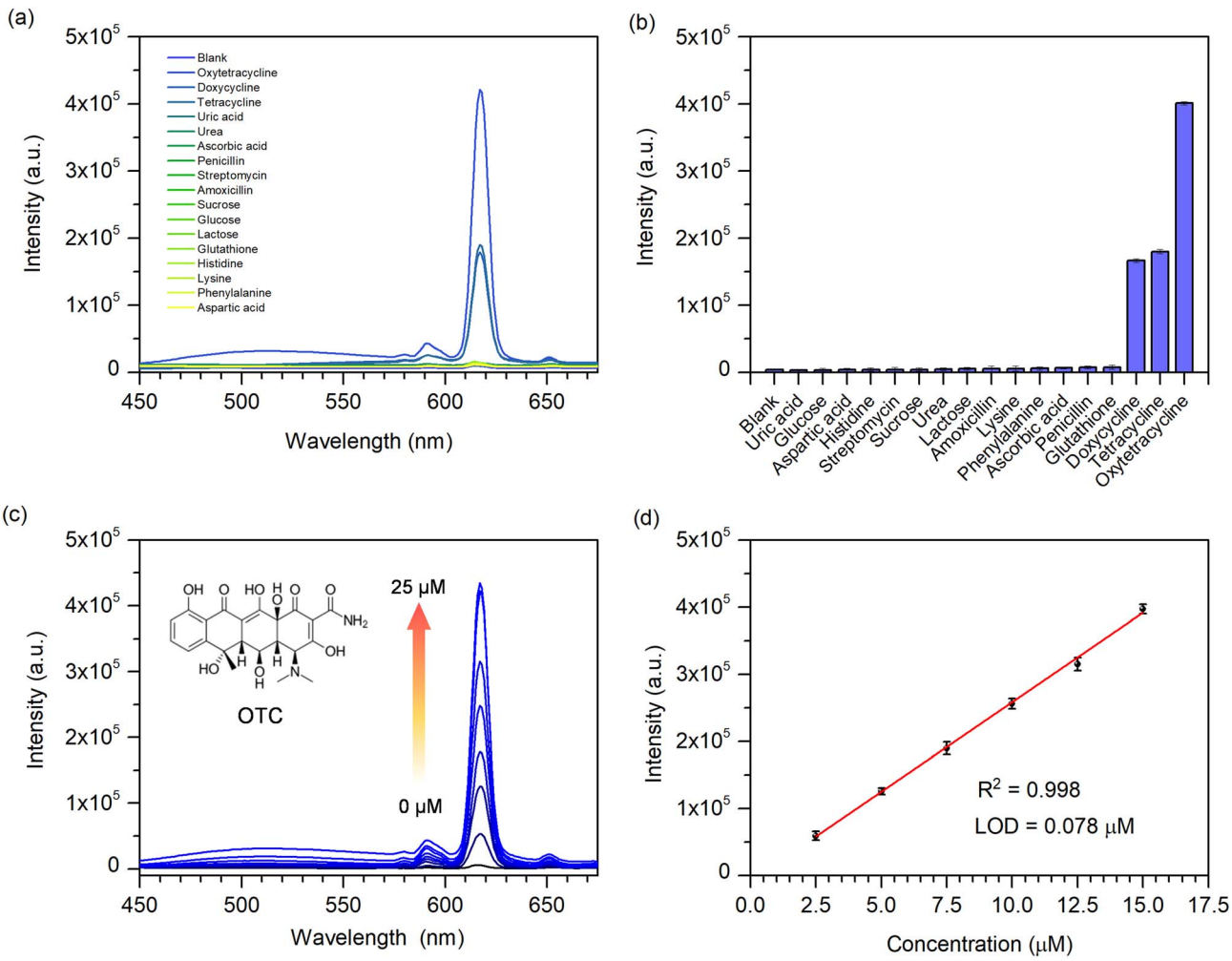

Fig. 3 (a) Fluorescent spectra and (b) comparison of the fluorescent intensity at 616 nm ($\lambda_{ex} = 368$ nm) for **Eu-MOF** after the addition of OTC and other chemicals (25 μM). (c) Emission spectra of **Eu-MOF** under different concentrations of OTC. (d) Linear plot of fluorescent intensity at 616 nm of **Eu-MOF** as a function with OTC concentrations.

concentrations of DOX and TC. Linear range of DOX concentration was found from 2.5 to 15.00 μM with a LOD of 0.201 μM, whereas TC linear range was 2.5–12.50 μM with a LOD of 0.225 μM (Fig. S6(b and d)‡). The obtained LOD values for OTC, DOX, and TC were less than the US Food and Drug Administration (FDA) permitted level of tetracycline antibiotics in milk, which was 0.67 μM.[5] The comparison of the fluorescence sensors used in TCs sensing is shown in Table S1.‡ When compared to other sensors, **Eu-MOF** demonstrated a comparatively low LOD and a relatively wide detection range. Moreover, in comparison with the Eu-In-BTEC, a MOF containing the same ligand as in the present study, which provides a low LOD of DOX, our proposed **Eu-MOF** still provides a comparatively low LOD and a wider detection range of DOX. In addition, the response time of **Eu-MOF** to OTC was investigated. In response to the addition of 50 μM OTC, the fluorescent of **Eu-MOF** increased rapidly after 1 min and subsequently changed slightly over the subsequent 40 min (Fig. S7(a and b)‡). This indicates that the sensor has a very quick response time. To further assess the selectivity of **Eu-MOF** toward OTC, the fluorescence responses to other antibiotics and potential interference chemicals were examined. As seen in Fig. S7(c and d),‡ OTC induces a strong fluorescence enhancement in the presence of antibiotics and other substances. According to these results, **Eu-MOF** could serve as a chemical sensor for the fast detection of OTC with high sensitivity, selectivity, and interference resistance.

3.4 Fluorescent enhancement mechanism

In order to explore the fluorescent enhancement mechanism, the PXRD pattern of **Eu-MOF** treated with OTC was investigated. It was found that the PXRD pattern of **Eu-MOF** in the presence of OTC was comparable to its as-prepared pattern, demonstrating that the fluorescence enhancement is not the result of a structural change (Fig. S8‡). The FT-IR spectrum of **Eu-MOF** was considerably changed following the incorporation of OTC. As shown in Fig. S9,‡ in **Eu-MOF** + OTC, the characteristic peak at 3210 cm^{-1}, which corresponds to O–H stretching in OTC, was diminished. The O–H bending peak of OTC was also shifted from 1447 to 1457 cm^{-1}. The C═O peaks of **Eu-MOF** + OTC at 1667 cm^{-1}, 1540 cm^{-1}, and 1379 cm^{-1} were weakened, illustrating that the carboxyl groups in **Eu-MOF** participate in the formation of complex between OTC and MOF *via* H-bonding. Moreover, the absorption spectra of **Eu-MOF**, OTC, and **Eu-MOF** + OTC were measured to investigate the complex formation between OTC and **Eu-MOF**. As seen in Fig. 4(a), two absorption peaks of OTC were observed at 275 and 355 nm. In comparison to the absorption spectra of **Eu-MOF**, **Eu-MOF** + OTC showed a novel absorption peak at 381 nm. The red shift of the absorption peak suggests the formation of a new complex between **Eu-MOF** and OTC. The interaction between OTC and the sensor may only take place at the surface of MOF. This is because the molecular size of OTC (1.32 × 0.70 nm)[42] is larger than the pore dimensions of **Eu-MOF** (1.04 × 0.99 nm), which may prevent OTC molecules from penetrating the polymer network.

To further explore the interaction between OTC and the sensor, XPS spectroscopy was performed to characterize the chemical state changes in **Eu-MOF** before and after the addition of OTC. As presented in Fig. 4(b), **Eu-MOF** showed three main peaks, Eu 3d, O 1s, and C 1s. After the addition of OTC to **Eu-MOF**, N 1s peaks were found at 400.19 eV and 399.17 eV, corresponding to H–N and C–N of OTC, respectively (inset Fig. 4(b)). The observed binding energy of N–H was higher than the values of 398.5–399.5 eV for typical amines and amides.[43] This is due to the loss of electron density around N atoms resulted from the interaction with Eu^{3+} in MOF by substitution the coordinated H_2O molecules.[18] Furthermore, two peaks of 3d orbital of Eu^{3+} in **Eu-MOF** + OTC present a slight shift to lower binding energy (Fig. 4(c)), suggesting the enhancement of the electron density at Eu^{3+} due to the coordination with amino functional group of OTC. Based on FT-IR and XPS analysis, H-bonding and the coordination of OTC to Eu^{3+} involve in the binding between OTC and the sensor. Upon excitation with suitable energy, the captured OTC could transfer the energy to Eu^{3+}, resulting in fluorescent enhancement. In addition to energy transfer, electron transfer plays an important role in fluorescent change. Time-dependent density-functional theory (TD-DFT) calculation at the B3LYP/6-31G* level was performed to investigate the HOMO (highest occupied molecular orbital) and LUMO (lowest unoccupied molecular orbital) of TCs and H_4btec ligand.[44–48] As shown in Fig. 4(d), all calculated LUMOs of tetracycline derivatives (OTC, TC, and DOX) are higher than the energy level of H_4btec ligand. This implies that the excited electron could be transferred from such antibiotics to ligand in the framework *via* photo-induced electron transfer process, supporting the antenna effect and resulting in fluorescent enhancement. In comparison to other tetracycline antibiotics, the LUMO energy level of OTC is closer to H_4btec ligand than those of TC and DOX. This might be a reason for the highest fluorescent enhancement induced by OTC. In addition, the observed differences in the response intensities induced by tetracycline antibiotics might be attributed to their different binding abilities with **Eu-MOF**. Considering the chemical structure, OTC has a higher hydroxyl functional group compared with TC and DOX (see Fig. S5‡). This leads to a higher number of hydrogen bond donors for binding with carboxyl groups in **Eu-MOF**. These interactions could improve the rigidity of the MOF structure, hence inhibiting radiationless relaxation routes *via* ligand movement to allow the highest fluorescent enhancement. According to these results, the enhancement effect of OTC on **Eu-MOF** is attributed to the coexistence of H-bonding and the coordination of OTC to Eu^{3+} that lead to energy transfer and photo-induced electron transfer processes. Furthermore, the pre-concentration effect of OTC could be induced by the specific interaction between the free carboxyl functional site and metal centre with OTC, improving the sensitivity of the sensor.

3.5 Turned-off detection of dihydrogen phosphate

In addition to the sensing of tetracycline antibiotics, the sensing ability of **Eu-MOF** for $H_2PO_4^-$ was explored. The fluorescence of the suspension of **Eu-MOF** in DI water was monitored (λ_{ex} = 254 nm) with the addition of 50 μM of various anions that include F^-, Cl^-, Br^-, I^-, NO_3^-, CO_3^{2-}, NO_2^-, CN^-,

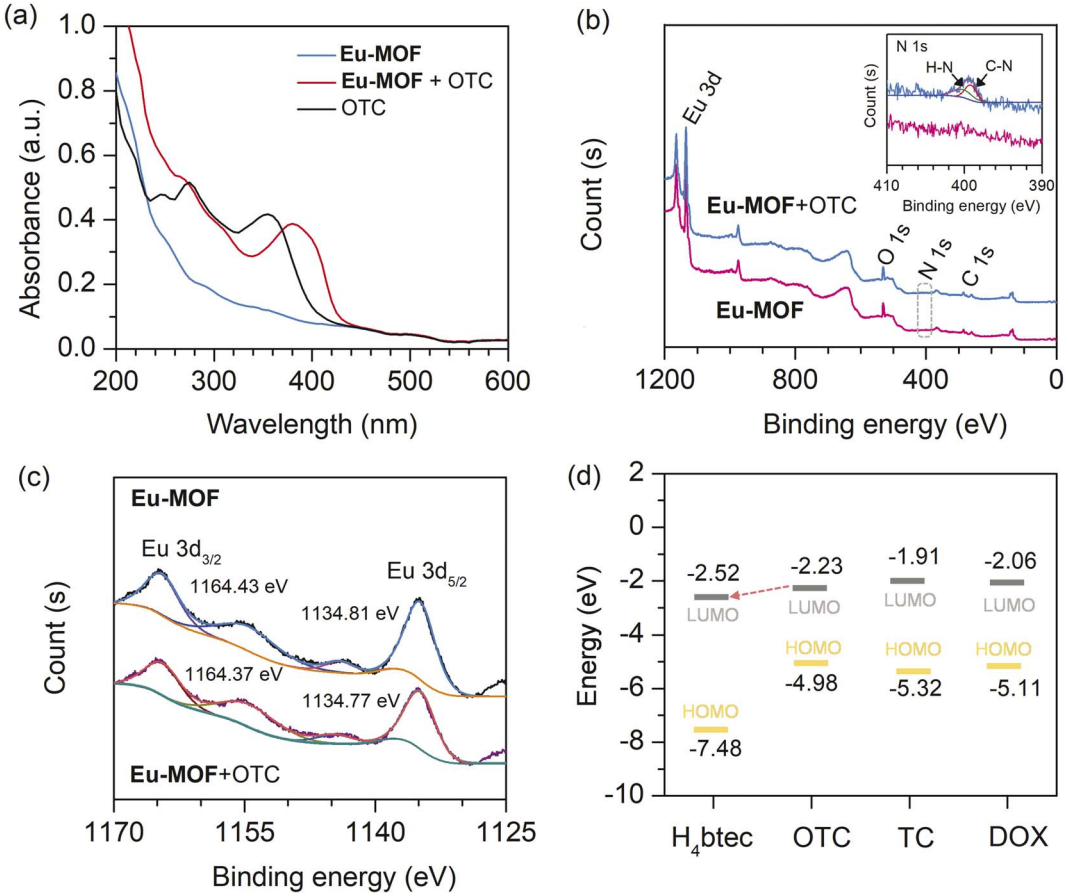

Fig. 4 (a) The absorption spectra of **Eu-MOF**, **Eu-MOF** + OTC, and OTC. XPS spectra of **Eu-MOF** before and after the addition of OTC: (b) full view (inset shows N 1s XPS spectrum of **Eu-MOF** with and without OTC) and (c) Eu 3d XPS spectrum (d) calculated energy level of HOMO (highest occupied molecular orbital) and LUMO (lowest unoccupied molecular orbital) for H_4btec ligand, OTC, TC, and DOX.

OAc^-, ClO_4^-, SO_4^{2-}, S^{2-}, and $H_2PO_4^-$ in term of sodium salts. In general, phosphates can exist as three different forms ($H_2PO_4^-$, HPO_4^{2-}, and PO_4^{3-}) depending on the pH of solution. The experimental pH of the solution for the sensing experiment is 6.70. The pK_2 of $H_2PO_4^-$ is 7.21.[28] As a result, with a pH of 6.70, the studied phosphate is predominantly in the form of $H_2PO_4^-$. As depicted in Fig. 5(a and b), the emission intensity at 616 nm of **Eu-MOF** was found to be strongly quenched by $H_2PO_4^-$ in comparison with other anions. This demonstrates the potential application for selective turn-off sensing of $H_2PO_4^-$ by **Eu-MOF**. In practical applications, a chemical sensor must possess not only great sensitivity and selectivity, but also an effective quick reaction time and anti-interference. The response time of **Eu-MOF** to $H_2PO_4^-$ was studied. Within 1 minute of the injection of 50 μM $H_2PO_4^-$, the fluorescence of **Eu-MOF** was sharply decreased and reached a plateau in about 30 min (Fig. S10(a and b)‡). Hence, the response time is quite short. As demonstrated in Fig. S10(c and d),‡ significant fluorescence quenching was detected when $H_2PO_4^-$ was added to the **Eu-MOF** solution containing interfering anions, indicating that the fluorescent quenching of the sensor stimulated by $H_2PO_4^-$ was barely affected by other anions. This indicates an excellent anti-interference capability of **Eu-MOF**. To investigate the quantitative detection of $H_2PO_4^-$, fluorescence quenching titration was performed with varied $H_2PO_4^-$ concentrations. As shown in Fig. 5(c), as the $H_2PO_4^-$ concentration increased, the fluorescence intensity of **Eu-MOF** gradually decreased. Fig. 5(d) displays the good linear relationship (R^2 = 0.996) between fluorescent intensity at 616 nm and $H_2PO_4^-$ concentration in the concentration range of 2.5–15 μM. The LOD of $H_2PO_4^-$ was found to be 0.70 μM calculated by the formula LOD = $3\sigma/S$. In addition, the quenching efficiency can be evaluated using the Stern–Volmer (SV) equation, $(I_0/I) = K_{SV}[Q] + 1$, (I_0 and I are the fluorescent intensities in the absence and presence of the analyte, respectively, K_{SV} is the quenching constant (M^{-1}), and $[Q]$ is the analyte concentration (μM)). According to the Stern–Volmer plot of **Eu-MOF** (Fig. S11‡), the linear relationship is obtained at concentrations of $H_2PO_4^-$ less than 10 μM, and the K_{SV} was found to be 7.242×10^4 M^{-1}. A nonlinear curve was obtained at higher concentrations. This indicates that the quenching process might be a combination of static and dynamic quenching processes. Moreover, the obtained LOD is far below the Environmental Protection Agency's (EPA) permitted phosphate limit for drinking water (5 mg L^{-1} or 52.6 μM).[9] As shown in Table S2,‡ the detection limit of $H_2PO_4^-$ by **Eu-MOF** is superior to that of multiple optical probes. In light of

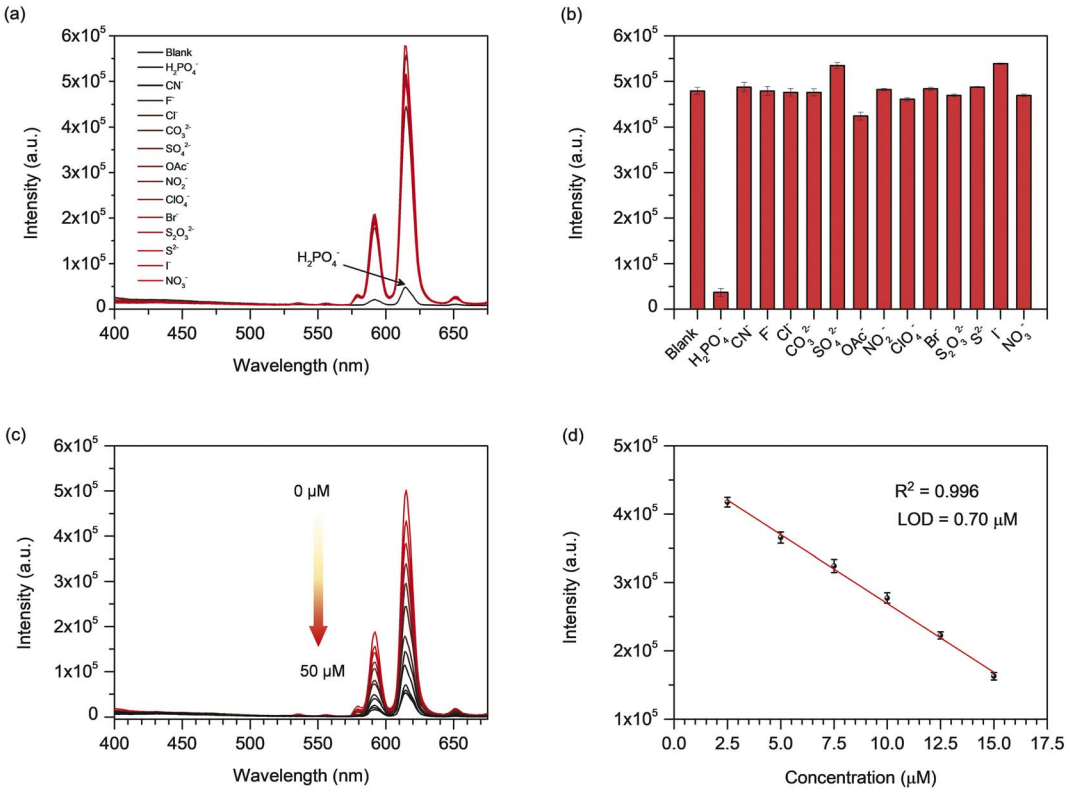

Fig. 5 (a) Fluorescent spectra and (b) comparison of the fluorescent intensity at 616 nm ($\lambda_{ex} = 254$ nm) for **Eu-MOF** after the addition of various anions (50 μM). (c) Emission spectra of **Eu-MOF** under different concentrations of $H_2PO_4^-$. (d) Linear plot of fluorescent intensity at 616 nm of **Eu-MOF** as a function with $H_2PO_4^-$ concentrations.

these results, **Eu-MOF** demonstrates a water-stable chemical sensor for the quick detection of $H_2PO_4^-$ anion with excellent sensitivity, selectivity, and interference resistance.

3.6 Fluorescent quenching mechanism

As shown in Fig. S8,‡ the main PXRD pattern of **Eu-MOF** treated with $H_2PO_4^-$ was similar to that of an untreated one, showing that the structure of MOF was maintained. This suggests that the quenching of fluorescence is not related to the structural disintegration of MOF. As shown in Fig. S12(a),‡ the FT-IR spectra revealed that the stretching frequency of the P–O bond was observed at 1068 cm^{-1} upon addition of $H_2PO_4^-$ in **Eu-MOF**. This suggested the incorporation of $H_2PO_4^-$ in the structure of **Eu-MOF**. In addition, as presented in Fig. S12(b),‡ stretching vibrations of carboxylic group in **Eu-MOF** + $H_2PO_4^-$ shows a little blue shift from 1379 to 1384 cm^{-1}, indicating that $H_2PO_4^-$ weakens the interaction between Eu^{3+} and organic ligands, resulting in the interruption of the energy transfer from the ligand to Eu^{3+}. XPS spectroscopy was also carried out to study the interaction between **Eu-MOF** and $H_2PO_4^-$. As depicted in Fig. 6(a), after being treated with $H_2PO_4^-$, a newly detected peak at around 190 eV can be attributed to the 2s orbital of the P element (inset Fig. 6(a)) while the binding energy of P 2p peak (132.9 eV) overlaps with a broad peak of the Eu 4d peak. Additionally, the O 1s spectra of **Eu-MOF** + $H_2PO_4^-$ are markedly different from those of the parent **Eu-MOF**. As depicted in (Fig. 6(b)), the O 1s spectra of bare **Eu-MOF** presents three peaks at 530.54 eV, 531.36 eV, and 533.02, belonging to Eu–O, Eu–OH, and O=C–O, respectively. In the presence of $H_2PO_4^-$, the deconvoluted O 1s spectra of **Eu-MOF** + $H_2PO_4^-$ has four peaks that correspond to O in O–C=O (533.69 eV), P–OH (532.20 eV), Eu–O (530.98 eV), and Eu–O–P and P=O (531.57 eV), respectively.[49,50] This evidences the incorporation of $H_2PO_4^-$ and the formation of Eu–O–P bond in **Eu-MOF**. According to the Eu 3d XPS data (Fig. 6(c)), the binding energy of Eu $3d_{3/2}$ and Eu $3d_{5/2}$ in **Eu-MOF** + $H_2PO_4^-$ was positively shifted in compared with the bare MOF (that for Eu $3d_{5/2}$ is from 1134.81 to 1135.20 eV, and that for Eu $3d_{3/2}$ is from 1164.43 to 1164.82 eV). This may be a result of phosphate groups interacting with the Eu^{3+} core in MOF. The lost electron density at the europium core, caused by the more electronegative P–O bonds, leads to an increase in 3d binding energy.[51] These experimental studies (FT-IR and XPS) demonstrated that the Eu–P–O bonds influence the coordination environment of the ligand with Eu^{3+}, resulting in a partial interruption of energy transfer between the organic ligand and metal center, leading to the decrease in fluorescence intensity. In addition to the more negative P–O bond, the hydrogen-bonding characteristics between $H_2PO_4^-$ and **Eu-MOF** may be the basis of the remarkable fluorescence quenching of **Eu-MOF** by $H_2PO_4^-$ over other anions. $H_2PO_4^-$ behaves as a hydrogen bond acceptor and donor in nature. In the pore of **Eu-MOF**, free carboxyl (–COOH) functional group composed of carbonyl (C=

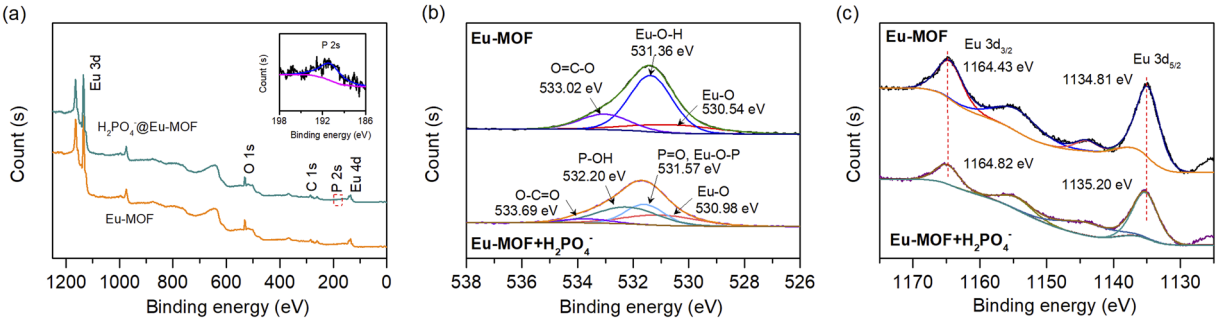

Fig. 6 XPS spectra of **Eu-MOF** before and after the addition of $H_2PO_4^-$: (a) full view XPS spectrum (inset shows P 2s XPS spectrum of **Eu-MOF** treated with $H_2PO_4^-$) (b) O 1s XPS spectrum and (c) Eu 3d XPS spectrum.

O) as a hydrogen bond acceptor and a hydroxyl group (–OH) as a hydrogen donor. Thus, it is possible that a small $H_2PO_4^-$ may enter the void and form hydrogen bonds with the –COOH functional site of **Eu-MOF**. This could also lead to intense adsorption of $H_2PO_4^-$, providing the pre-concentration effect and bringing $H_2PO_4^-$ get close to Eu^{3+} centre where it can interact with, and result in an increase in detection sensitivity.

3.7 Application to real samples

The spike-and-recovery studies were carried out to demonstrate the practical implementation of the proposed sensor for OTC. The samples used were milk, chicken breast, and honey. The real samples were prepared according to the experimental method, and then different concentrations (5 μM and 10 μM) of OTC were added to the selected samples. As shown in Table 1, OTC was not detected in the control. The spiking recovery of the **Eu-MOF** sensor is in the range of 87.00–109.03%, and the relative standard deviations (RSDs) were less than 10% ($n = 3$). Additionally, **Eu-MOF** was applied to detect $H_2PO_4^-$ in drinking water and lake water samples in Khon Kaen, Thailand. As presented in Table 1, the added $H_2PO_4^-$ solution could be determined with satisfactory recoveries ranging from 84.90 to 90.00% with the RSDs less than 10.0% ($n = 3$). These findings demonstrate the viability and dependability of the **Eu-MOF** for precise determination of OTC and $H_2PO_4^-$ in actual samples.

Table 1 Analysis results of OTC and $H_2PO_4^-$ in real samples by **Eu-MOF** ($n = 3$)[a]

Target molecule	Samples	Spiked (μM)	Found (μM)	Recovery ± RSD (%)
OTC	Whole fresh milk	0.00	n.d.	—
		5.00	5.46 ± 0.25	109.03 ± 4.56
		10.00	10.45 ± 0.63	104.46 ± 6.02
	UHT milk	0.00	n.d.	—
		5.00	5.35 ± 0.12	106.90 ± 2.29
		10.00	8.73 ± 0.50	87.24 ± 5.78
	Chicken breast	0.00	n.d.	—
		5.00	4.98 ± 0.24	99.50 ± 4.92
		10.00	8.70 ± 0.36	87.00 ± 4.09
	Honey	0.00	n.d.	—
		5.00	4.91 ± 0.22	98.20 ± 4.45
		10.00	9.23 ± 0.79	94.79 ± 5.34
$H_2PO_4^-$	Drinking water	0.00	n.d.	—
		5.00	4.27 ± 0.32	85.33 ± 7.73
		10.00	9.00 ± 0.51	90.00 ± 5.57
	Lake water	0.00	n.d.	—
		5.00	4.45 ± 0.25	89.00 ± 5.62
		10.00	8.49 ± 0.38	84.90 ± 4.51

[a] n.d. = not detectable (less than LOD).

3.8 Identification of latent fingerprint fluorescent quenching mechanism

As fingerprints are such a reliable representation of personal information, they are essential at crime scenes. It is therefore crucial to provide a reliable method for detecting latent fingerprints (LFPs). Motivated by the strong red fluorescence and the prospect of expanding applicability of **Eu-MOF**, it was applied for the visualization of LFPs. A simple procedure for fluorescent visualization of LFPs is illustrated in Fig. 7(a). The details and patterns of undeveloped fingerprints on the glass slide could not be clearly observed under day light and 365 nm UV light as can be seen in Fig. 7(b). Ideally, the LFPs developing technology should incorporate all of the distinctive fingerprint characteristics from level 1 (overall fingerprint shape, core point, *etc.*), level 2 (bifurcation, termination, crossover, *etc.*) to level 3 (scar, sweat pore, *etc.*).[52,53] After applying the **Eu-MOF** powder to the substrate, the pattern feature (level 1) of the developed fingerprint was immediately and clearly observed under UV light with apparently higher contrast between the fluorescent ridges and non-fluorescent furrow (Fig. 7(c)). On top of that, the enlarged fingerprint also reveals the information at the level 1 (core point) and level 2 (termination, bifurcation, crossover) with the naked eye. Surprisingly, level 3 details (scar and sweat pore) can also be distinguished without post-treatment method (Fig. 7(d)). These level 2 and 3 characteristics are sufficient for fingerprint analysis since they contain a significant amount of individual information. Photostability and long-term stability are vital factors for evaluating the ability of **Eu-MOF** for LFPs detection in actual scenarios. The photographs of LFPs developed with **Eu-MOF** under UV light were shown in Fig. S13.‡ Under 365 nm UV light for 7 hours, high-contrast fluorescence images of LFPs can be clearly seen,

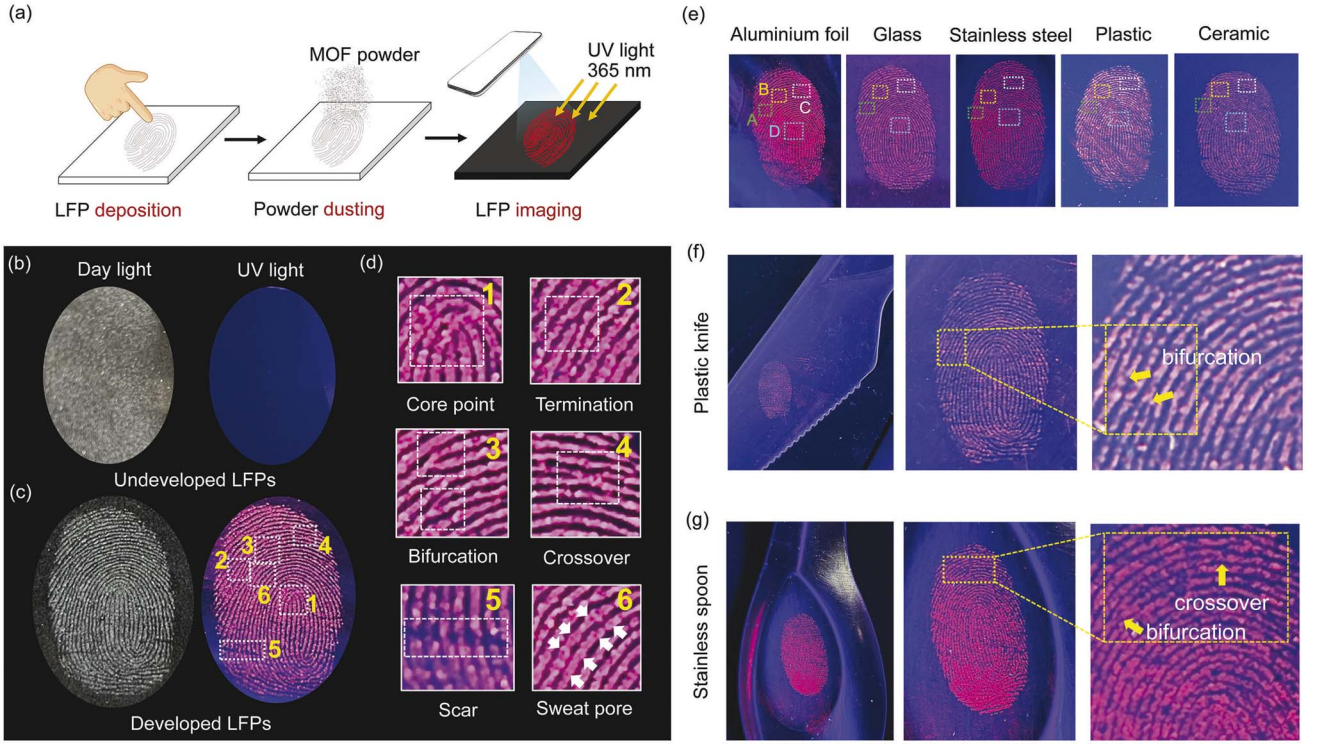

Fig. 7 (a) Steps for using MOF powders for fluorescent LFPs visualization. Photographs of undeveloped (b) and developed (c) latent fingerprints on glass slide under day light and UV light (365 nm). (d) Enlarged images showing level 1–3 features of fingerprint details as marked in (c) including (1) core point, (2) termination, (3) bifurcation, (4) crossover, (5) scar, and (6) sweat pore. (e) Photographs of latent fingerprints developed with **Eu-MOF** materials on different substrates under UV light. The marked areas show (A) termination, (B) bifurcation, (C) crossover, and (D) core point. Photographs of latent fingerprints developed with **Eu-MOF** on the surface of a plastic knife (f) and a stainless spoon (g) under UV light. The left and middle sets of images show visualized latent fingerprints under 365 nm UV light. The right set of images show bifurcation and crossover on the latent fingerprints.

demonstrating the photostability of **Eu-MOF**. Furthermore, 30 day-old LFPs can still be observed clearly without loss of clarity, indicating the good long-term stability of **Eu-MOF** (Fig. S14‡). The above results indicated that that **Eu-MOF** could serve as an efficient tool for investigating the biological features of individual fingerprints. Moreover, the fluorescent imaging of developed LFPs on various substrates commonly used in daily life, including aluminium foil, glass, stainless steel, plastic, and ceramic was also demonstrated. As shown in Fig. 7(e), the fingerprint details on aluminium foil were clearly observed by the naked eye and displayed distinct features of (A) termination, (B) bifurcation, (C) crossover, and (D) core point (Fig. S15‡). Similar good results could also be observed distinctly on another substrate. To demonstrate the practicality of the **EuMOF** for the identification of LFPs as the "weight of evidence" in forensic science, we conducted developing experiments on the surface of real forensic samples such as plastic knife and stainless spoon. As illustrated in Fig. 7(f) and (g), the fingerprint patterns can be clearly observed and all the fingermarks show well-defined details, indicating that **Eu-MOF** can effectively recognize the individual identity at the crime scene. This is due primarily to the intense red fluorescence of the **Eu-MOF** may reduce background interference. The interaction between **Eu-MOF** and fingerprints is attributed to hydrophobic interaction between the π-conjugated ligand on **Eu-MOF** and the fatty components (wax esters, fatty acids, squalene, and cholesterol) of LFPs that causes **Eu-MOF** to engage with the fingerprint ridges as opposed to the furrows.[54] Additionally, the interaction between the carboxyl groups of some compounds in fingerprint residues (fatty acids, lactic acid, and other substances) and the hydroxyl groups on carboxyl groups in **Eu-MOF** could participate in the specific binding and improve LFPs identification sensitivity.[55] Because of its good fluorescence and specific interactions, **Eu-MOF** could therefore be employed to develop latent fingerprints from level 1 to level 3 with high sensitivity, anti-background interference, and simplicity of use.

4. Conclusion

A water-stable **Eu-MOF** decorated with free carboxyl functional groups to recognize the guest molecules was successfully constructed *via* a one-step hydrothermal method. **Eu-MOF** was demonstrated for the first time as a dual-responsive fluorescent sensor, a turn-on probe and a turn-off probe for tetracycline antibiotics and dihydrogen phosphate, respectively. Low limits of detection of OTC, TC, and DOX were obtained at 78 nM, 225 nM, and 201 nM, respectively. The enhancement effect of tetracycline antibiotics on **Eu-MOF** is based upon the hydrogen

bond and coordination interactions that result in energy and electron transfer from antibiotics to MOF. In addition, **Eu-MOF** could sensitively and selectively detect $H_2PO_4^-$ in aqueous media with a low limit of detection of 0.70 μM. The fluorescent quenching is attributed to the interference of the antenna process upon **Eu-MOF** interacted with $H_2PO_4^-$. Importantly, the presented sensor has been applied for the determination of OTC and $H_2PO_4^-$ in real samples (milk, chicken breast, honey, and water samples) with satisfactory recoveries. According to the findings, **Eu-MOF** could be employed as a promising sensory material for the effective detection of antibiotics and anion. Because of this, our work may contribute to the design and development of an excellent MOF-based dual-responsive (turn-on and turn-off) fluorescence sensor, which could be used in the fields of food safety and environmental protection. More interestingly, the development of latent fingerprints using **Eu-MOF** allowed for reliable imaging of LPF features at levels 1 through 3 with high contrast, anti-background interference, and ease-of-use. This proposed **Eu-MOF** is expected to have wide-ranging applications in LFPs visualization.

Conflicts of interest

There are no conflicts to declare.

Acknowledgements

This work was financially supported by the National Research Council of Thailand (NRCT), Grant no. N41A640144 and the Fundamental Fund of Khon Kaen University through the National Science, Research and Innovation Fund, Thailand. We would like to thank Prof. Dr Supalax Srijaranai for providing antibiotics.

References

1 C. Lu, Z. Tang, C. Liu, L. Kang and F. Sun, Magnetic nano bead- based competitive enzyme-linked aptamer assay for the analysis of oxytetracycline in food, *Anal. Bioanal. Chem.*, 2015, **407**, 4155–4163.

2 X. Xing, L. Huang, S. Zhao, J. Xiao and M. Lan, S,N-Doped carbon dots for tetracyclines sensing with a fluorometric spectral response, *Microchem. J.*, 2020, **157**, 105065.

3 Y. Xu, C. Lu, Y. Sun, Y. Shao, Y. Cai, Y. Zhang, J. Miao and P. Miao, A colorimetric aptasensor for the antibiotics oxytetracycline and kanamycin based on the use of magnetic beads and gold nanoparticles, *Microchim. Acta*, 2018, **185**, 548.

4 L. A. Hamilton and A. J. Guarascio, Tetracycline allergy, *Pharmacy*, 2019, **7**, 104.

5 C. Li, L. Zhu, W. Yang, X. He, S. Zhao, X. Zhang, W. Tang, J. Wang, T. Yue and Z. Li, Amino-functionalized Al-MOF for fluorescent detection of tetracyclines in milk, *J. Agric. Food Chem.*, 2019, **67**, 1277–1283.

6 R. Hetz, E. Beeler, A. Janoczkin, S. Kiers, L. Li, B. B. Willard, M. S. Razzaque and P. He, Excessive inorganic phosphate burden perturbed intracellular signaling: quantitative proteomics and phosphoproteomics analyses, *Front. Nutr.*, 2022, **8**, 765391.

7 C. Warwick, A. Guerreiro and A. Soares, Sensing and analysis of soluble phosphates in environmental samples: a review, *Biosens. Bioelectron.*, 2013, **41**, 1–11.

8 J. M. Estela and V. Cerdà, Flow analysis techniques for phosphorus: an overview, *Talanta*, 2005, **66**, 307–331.

9 K. Naskar, A. K. Bhanja, S. Paul, K. Pal and C. Sinha, Trace quantity detection of $H_2PO_4^-$ by fluorescent metal-organic framework (F-MOF) and bioimaging study, *Cryst. Growth Des.*, 2020, **20**, 6453–6460.

10 P. Li, L. Dong, H. Jin, J. Yang, Y. Tu, C. Wang and Y. He, Fluorescence detection of phosphate in an aqueous environment by an aluminum-based metal–organic framework with amido functionalized ligands, *Front. Environ. Sci. Eng.*, 2022, **16**, 159.

11 X.-D. Zhu, K. Zhang, Y. Wang, W.-W. Long, R.-J. Sa, T.-F. Liu and J. Lü, Fluorescent metal-organic framework (MOF) as a highly sensitive and quickly responsive chemical sensor for the detection of antibiotics in simulated wastewater, *Inorg. Chem.*, 2018, **57**, 1060–1065.

12 F. G. Moscoso, J. Almeida, A. Sousaraei, T. Lopes-Costa, A. M. G. Silva, J. Cabanillas-Gonzalez, L. Cunha-Silva and J. M. Pedrosa, A lanthanide MOF immobilized in PMMA transparent films as a selective fluorescence sensor for nitroaromatic explosive vapours, *J. Mater. Chem. C*, 2020, **8**, 3626–3630.

13 J. Li, S. Yuan, J.-S. Qin, J. Pang, P. Zhang, Y. Zhang, Y. Huang, H. F. Drake, W. R. Liu and H.-C. Zhou, Stepwise assembly of turn-on fluorescence sensors in multicomponent metalorganic frameworks for *in vitro* cyanide detection, *Angew. Chem., Int. Ed.*, 2020, **59**, 9319–9323.

14 L.-J. Han, Y.-J. Kong, G.-Z. Hou, H.-C. Chen, X.-M. Zhang and H.-G. Zheng, A europium-based MOF fluorescent probe for efficiently detecting malachite green and uric acid, *Inorg. Chem.*, 2020, **59**, 7181–7187.

15 H. Yu, Q. Liu, J. Li, Z.-M. Su, X. Li, X. Wang, J. Sun, C. Zhou and X. Hu, A dual-emitting mixed-lanthanide MOF with high water-stability for ratiometric fluorescence sensing of Fe^{3+} and ascorbic acid, *J. Mater. Chem. C*, 2021, **9**, 562–568.

16 G.-D. Wang, Y.-Z. Li, W.-J. Shi, B. Zhang, L. Hou and Y.-Y. Wang, A robust cluster-based Eu-MOF as multi-functional fluorescence sensor for detection of antibiotics and pesticides in water, *Sens. Actuators, B*, 2021, **331**, 129377.

17 Y. Zhou, Q. Yang, D. Zhang, N. Gan, Q. Li and J. Cuan, Detection and removal of antibiotic tetracycline in water with a highly stable luminescent MOF, *Sens. Actuators, B*, 2018, **262**, 137–143.

18 Q. Liu, D. Ning, W.-J. Li, X.-M. Du, Q. Wang, Y. Li and W.-J. Ruan, Metal–organic framework-based fluorescent sensing of tetracycline-type antibiotics applicable to environmental and food analysis, *Analyst*, 2019, **144**, 1916–1922.

19 Q. Wang, X. Li, K. Yang, S. Zhao, S. Zhu, B. Wang, J. Yi, Y. Zhang, X. Song and M. Lan, Carbon dots and Eu^{3+} hybrid based ratiometric fluorescent probe for

oxytetracycline detection, *Ind. Eng. Chem. Res.*, 2022, **61**, 5825–5832.

20 Y. Li, Y. Wang, P. Du, L. Zhang, Y. Liu and X. Lu, Fabrication of carbon dots@hierarchical mesoporous ZIF-8 for simultaneous ratiometric fluorescence detection and removal of tetracycline antibiotics, *Sens. Actuators, B*, 2022, **358**, 131526.

21 Y. Zhao, Q. Wang, H. Wang, H. Zhangsun, X. Sun, T. Bu, Y. Liu, W. Wang, Z. Xu and L. Wang, Europium-based metalorganic framework containing characteristic metal chains: a novel turn-on fluorescence sensor for simultaneous high performance detection and removal of tetracycline, *Sens. Actuators, B*, 2021, **334**, 129610.

22 J. Chen, F. Xu, Q. Zhang, S. Li and X. Lu, Tetracycline antibiotics and NH^{4+} detection by Zn-organic framework fluorescent probe, *Analyst*, 2021, **146**, 6883–6892.

23 L. Yu, H. Chen, J. Yue, X. Chen, M. Sun, J. Hou, K. A. Alamry, H. M. Marwani, X. Wang and S. Wang, Europium metal–organic framework for selective and sensitive detection of doxycycline based on fluorescence enhancement, *Talanta*, 2020, **207**, 120297.

24 W. Sun, J. Wang, G. Zhang and Z. Liu, A luminescent terbium MOF containing uncoordinated carboxyl groups exhibits highly selective sensing for Fe^{3+} ions, *RSC Adv.*, 2014, **4**, 55252–55255.

25 J. Dong, X.-D. Zhang, X.-F. Xie, F. Guo and W.-Y. Sun, Amino group dependent sensing properties of metal–organic frameworks: selective turn-on fluorescence detection of lysine and arginine, *RSC Adv.*, 2020, **10**, 37449–37455.

26 K. S. Asha, R. Bhattacharjee and S. Mandal, Complete transmetalation in a metal-organic framework by metal ion metathesis in a single crystal for selective sensing of phosphate ions in aqueous media, *Angew. Chem., Int. Ed.*, 2016, **55**, 11528–11532.

27 R. Dalapati and S. Biswas, Post-synthetic modification of a metal–organic framework with fluorescent-tag for dual naked eye sensing in aqueous medium, *Sens. Actuators, B*, 2017, **239**, 759–767.

28 S. Jindal and J. N. Moorthy, Zwitterionic luminescent 2D metal organic framework nanosheets (LMONs): selective turn-on fluorescence sensing of dihydrogen phosphate, *Inorg. Chem.*, 2022, **61**, 3942–3950.

29 R. Zou, Y. Yu, H. Pan, P. Zhang, F. Cheng, C. Zhang, S. Chen, J. Chen and R. Zeng, Cross-linking induced emission of polymer micelles for high-contrast visualization level 3 details of latent fingerprints, *ACS Appl. Mater. Interfaces*, 2022, **14**, 16746–16754.

30 B. Shin-Il Kim, Y.-J. Jin, M. A. Uddin, T. Sakaguchi, H. Y. Woo and G. Kwak, Surfactant chemistry for fluorescence imaging of latent fingerprints using conjugated polyelectrolyte nanoparticles, *Chem. Commun.*, 2015, **51**, 13634–13637.

31 B.-P. Jiang, Y.-X. Yu, X.-L. Guo, Z.-Y. Ding, B. Zhou, H. Liang and X.-C. Shen, White-emitting carbon dots with long alkyl chain structure: effective inhibition of aggregation caused quenching effect for label-free imaging of latent fingerprint, *Carbon*, 2018, **128**, 12–20.

32 Q. Wang and W.-M. Zhao, Optical methods of antibiotic residues detections: a comprehensive review, *Sens. Actuators, B*, 2018, **269**, 238–256.

33 J. Lee, C. W. Lee and J.-M. Kim, A magnetically responsive polydiacetylene precursor for latent fingerprint analysis, *ACS Appl. Mater. Interfaces*, 2016, **8**, 6245–6251.

34 H. Chen, R.-l. Ma, Y. Chen and L.-J. Fan, Fluorescence development of latent fingerprint with conjugated polymer nanoparticles in aqueous colloidal solution, *ACS Appl. Mater. Interfaces*, 2017, **9**, 4908–4915.

35 Y. Jiang, Y. Huang, X. Shi, Z. Lu, J. Ren, Z. Wang, J. Xu, Y. Fan and L. Wang, Eu-MOF and its mixed-matrix membranes as a fluorescent sensor for quantitative ratiometric pH and folic acid detection, and visible fingerprint identifying, *Inorg. Chem. Front.*, 2021, **8**, 4924–4932.

36 K. Yi, H. Li, X. Zhang and L. Zhang, Designed Tb(III)-functionalized MOF-808 as visible fluorescent probes for monitoring bilirubin and identifying fingerprints, *Inorg. Chem.*, 2021, **60**, 3172–3180.

37 M. Kurjogi, Y. H. Issa Mohammad, S. Alghamdi, M. Abdelrahman, P. Satapute and S. Jogaiah, Detection and determination of stability of the antibiotic residues in cow's milk, *PLoS One*, 2019, **14**, e0223475.

38 N. Gissawong, S. Boonchiangma, S. Mukdasai and S. Srijaranai, Vesicular supramolecular solvent-based microextraction followed by high performance liquid chromatographic analysis of tetracyclines, *Talanta*, 2019, **200**, 203–211.

39 B. Lin, T. Zhang, X. Xin, D. Wu, Y. Huang, Y. Liu, Y. Cao, M. Guo and Y. Yu, Europium(III) modified silicone nanoparticles for ultrasensitive visual determination of tetracyclines by employing a fluorescence color switch, *Microchim. Acta*, 2019, **186**, 442.

40 T. Wiwasuku, A. Chuaephon, U. Habarakada, J. Boonmak, T. Puangmali, F. Kielar, D. J. Harding and S. Youngme, A water-stable lanthanide-based MOF as a highly sensitive sensor for the selective detection of paraquat in agricultural products, *ACS Sustainable Chem. Eng.*, 2022, **10**, 2761–2771.

41 R. Feyisa Bogale, J. Ye, Y. Sun, T. Sun, S. Zhang, A. Rauf, C. Hang, P. Tian and G. Ning, Highly selective and sensitive detection of metal ions and nitroaromatic compounds by an anionic europium(III) coordination polymer, *Dalton Trans.*, 2016, **45**, 11137–11144.

42 R. Rodríguez-Dorado, A. M. Carro, I. Chianella, K. Karim, A. Concheiro, R. A. Lorenzo, S. Piletsky and C. Alvarez-Lorenzo, Oxytetracycline recovery from aqueous media using computationally designed molecularly imprinted polymers, *Anal. Bioanal. Chem.*, 2016, **408**, 6845–6856.

43 X. Cao and R. J. Hamers, Silicon surfaces as electron acceptors: dative bonding of amines with Si(001) and Si(111) surfaces, *J. Am. Chem. Soc.*, 2001, **123**, 10988–10996.

44 W. J. Hehre, R. Ditchfield and J. A. Pople, Self-consistent molecular orbital methods. XII. Further extensions of Gaussian type basis sets for use in molecular orbital studies of organic molecules, *Chem. Phys.*, 1972, **56**, 2257–2261.

45 P. C. Hariharan and J. A. Pople, The influence of polarization functions on molecular orbital hydrogenation energies, *Theor. Chim. Acta*, 1973, **28**, 213–222.
46 A. D. Becke, Density functional thermochemistry. III. The role of exact exchange, *J. Chem. Phys.*, 1993, **98**, 5648–5652.
47 K. Kim and K. Jordan, Comparison of density functional and MP2 calculations on the water monomer and dimer, *J. Chem. Phys.*, 1994, **98**, 10089–10094.
48 K. Raghavachari, Perspective on Density functional thermochemistry. III. The role of exact exchange, *Theor. Chem. Acc.*, 2000, **103**, 361–363.
49 X. Zhu, B. Li, J. Yang, Y. Li, W. Zhao, J. Shi and J. Gu, Effective adsorption and enhanced removal of organophosphorus pesticides from aqueous solution by Zr-based MOFs of UiO-67, *ACS Appl. Mater. Interfaces*, 2015, **7**, 223–231.
50 Y. Wu, S. Zheng, Y. Ye, H. Guo and F. Yang, Crown-ether bridging bis-diphenylacrylonitrile macrocycle: the effective fluorescence sensor for oxytetracycline, *J. Photochem. Photobiol., A*, 2021, **412**, 113219.
51 Z. Li, Z. Zhan, Y. Jia, Z. Li and M. Hu, A water-stable europium-MOF as a multifunctional luminescent sensor for some inorganic ions and dichloromethane molecule, *J. Ind. Eng. Chem.*, 2021, **97**, 180–187.
52 X.-Y. Dong, X.-Q. Niu, Z.-Y. Zhang, J.-S. Wei and H.-M. Xiong, Red fluorescent carbon dot powder for accurate latent fingerprint identification using an artificial intelligence program, *ACS Appl. Mater. Interfaces*, 2020, **12**, 29549–29555.
53 Y.-L. Wang, C. Li, H.-Q. Qu, C. Fan, P.-J. Zhao, R. Tian and M.-Q. Zhu, Real-time fluorescence *in situ* visualization of latent fingerprints exceeding level 3 details based on aggregation induced emission, *J. Am. Chem. Soc.*, 2020, **142**, 7497–7505.
54 A. H. Malik, A. Kalita and P. K. Iyer, Development of well-preserved, substrate-versatile latent fingerprints by aggregation-induced enhanced emission-active conjugated polyelectrolyte, *ACS Appl. Mater. Interfaces*, 2017, **9**, 37501–37508.
55 D. Peng, X. Wu, X. Liu, M. Huang, D. Wang and R. Liu, Color tunable binuclear (Eu, Tb) nanocomposite powder for the enhanced development of latent fingerprints based on electrostatic interactions, *ACS Appl. Mater. Interfaces*, 2018, **10**, 32859–32866.